Comparative X-ray Diffraction Study of Two Liquid Crystalline Compounds with Chiral Centers Based on (S)-(+)-2-Octanol and (S)-(+)-3-Octanol

A. Deptuch[a,*], A. Lelito[b], B. Sęk[c] and M. Urbańska[d]

[a]*Institute of Nuclear Physics, Polish Academy of Sciences, Radzikowskiego 152, PL-31342 Kraków, Poland*
[b]*Faculty of Materials Engineering and Physics, Cracow University of Technology, Podchorążych 1, PL-30084 Kraków, Poland*
[c]*Faculty of Physics and Applied Computer Science, AGH University of Kraków, Reymonta 19, PL-30059 Kraków, Poland*
[d]*Institute of Chemistry, Military University of Technology, Kaliskiego 2, PL-00908 Warsaw, Poland*

Received: 11.03.2024 & Accepted: 23.04.2024

Doi: 10.12693/APhysPolA.146.79 *e-mail: aleksandra.deptuch@ifj.edu.pl

The structure of the antiferroelectric smectic C_A^* phase is investigated for two liquid crystals with almost identical molecular structures, except for chiral centers. The X-ray diffraction results determined the crystal unit cell parameters, smectic layer spacing, average distance within layers, and correlation length of the short-range positional order. The coefficients of thermal expansion are determined for the crystal phases. The molecular modeling with the semi-empirical PM7 method and density functional theory calculations with the def2TZVPP basis set and B3LYP-D3(BJ) functional are applied to determine the tilt angle of molecules from the experimental smectic layer spacing. The most probable conformations are then selected based on a comparison with the tilt angle measured by the electro–optic method, known from the previous results. In the most suitable molecular models, the chiral chain makes an approximately 90° angle with the molecular core, and some fragments in the fluorinated part of the achiral terminal chain are in the *gauche* conformation.

topics: X-ray diffraction, smectic liquid crystals, layer spacing, tilt angle

1. Introduction

The smectic phases are liquid crystalline (LC) phases characterized by the lamellar order. The lamellar order is quasi-long-range for the simplest smectic phases, and the positional order within the smectic layers is only short-range. In the smectic A (SmA) phase, the average tilt angle Θ of molecules relative to the layer normal is zero, while in the smectic C (SmC) phase, $\Theta \neq 0$. There are a few types of the SmC phase, including the synclinic, default SmC, and anticlinic SmC_A phases. In the latter, the tilt angle has an opposite sign in neighboring layers. The SmC^* and SmC_A^* phases, where * means that they are formed of chiral molecules, can show, respectively, the ferro- and antiferroelectric properties in certain conditions, corresponding to bistable and tristable switching under the influence of the electric field [1–3]. Particularly interesting are the LC compounds forming the SmC_A^* phase with a high tilt angle close to 45°, where the chevron defect in the LC alignment does not cause light leakage in the dark state of a display [4, 5].

The smectic layer spacing d, which can be obtained using the X-ray diffraction (XRD) method, is correlated with the tilt angle Θ. Determining the tilt angle from the XRD results and calculating molecular size using molecular modeling is not straightforward because the shapes of mesogenic molecules often deviate from the ideal rod. Consequently, there is a difference between the tilt of the molecular core (corresponding to the genuine tilt angle Θ measured by the electro-optic method) and the overall tilt of a molecule (referred to as the steric tilt angle) [6–8]. The formula for the tilt angle, which results from these considerations, is as follows

$$\Theta = \arccos(d/L) + \delta\Theta, \tag{1}$$

where L is the molecular length, and $\delta\Theta$ is the shape parameter. For a rod-like molecule, $\delta\Theta = 0$, while for non-linear molecules, this parameter can even

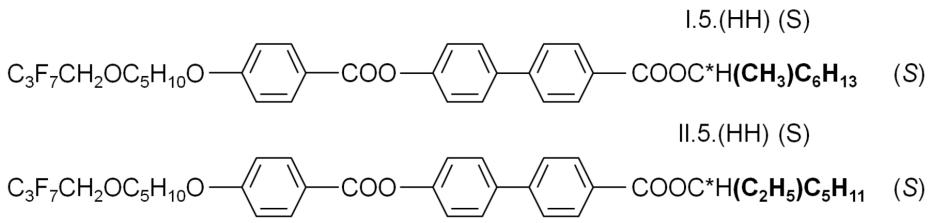

Fig. 1. Molecular formulas of I.5.(HH) (S) and II.5.(HH) (S).

exceed 20° [8]. It is necessary to test several molecular conformations to find the one that enables the best reproduction of the tilt angle measured by the electro-optic method [6–8]. In our previous papers and in the literature, various conformations are taken into account, including the more extended hockey-stick conformations [8–10] and more bent (C-shaped, zig–zag) ones [8, 10–12]. Knowledge of the most likely conformations can facilitate, e.g., the interpretation of the infrared (IR) spectra, the analysis of which usually involves the density functional theory (DFT) calculations of the intra-molecular vibrations [10, 11].

This work presents a comparative study of two chiral LC compounds. These compounds are (S)-4'-(1-methylheptylcarbonyl)biphenyl-4-yl 4-[5-(2,2,3,3,4,4,4-heptafluorobutoxy)pentyl-1-oxy]benzoate, abbreviated as I.5.(HH) (S) or 3F5HPhH6 (the first notation is further used) and (S)-4'-(1-ethylhexyloxycarbonyl)biphenyl-4-yl 4-[5-(2,2,3,3,4,4,4-heptafluorobutoxy)pentyl-1-oxy] benzoate, abbreviated as II.5.(HH) (S). The molar mass of these compounds is the same, and their molecular structures are almost identical (Fig. 1). The only difference is in the chiral center, based on (S)-(+)-2-octanol and (S)-(+)-3-octanol for I.5.(HH) (S) and II.5.(HH) (S), respectively. They both exhibit the antiferroelectric smectic C_A^* phase with a high tilt angle approaching 45° [13]; they are, therefore, promising components for orthoconic LC mixtures suitable for displays [4, 5]. The previous experimental results indicate that both these compounds form a glass of a smectic phase: I.5.(HH) (S) of the hexatic smectic X_A^* phase (SmI_A^* or SmF_A^*) for cooling rates $\geq$ 5 K/min [14] and II.5.(HH) (S) of the antiferroelectric SmC_A^* phase for cooling rates $\geq$ 2 K/min [15]. The fact that these compounds can be easily supercooled is another feature that makes them good for application in LC mixtures, where the observed range of the smectic phase should be as wide as possible.

The aim of this paper is analysis of the XRD patterns of I.5.(HH) (S) and II.5.(HH) (S) collected as a function of temperature. The structural parameters of the crystal, smectic, and isotropic liquid phases are obtained and discussed in relation to the results from other experimental methods published in [14, 15]. Then, the molecular models of I.5.(HH) (S) and II.5.(HH) (S) from the same set of conformations, optimized by the DFT method, are tested to determine the tilt angle from (1). The conformations, which give the tilt angle consistent with the tilt measured by the electro-optic method [13], are supposed to be the most probable conformations exhibited by molecules in the SmC_A^* phase.

2. Experimental and computational details

The synthetic route of (S)-4'-(1-methylheptylcarbonyl)biphenyl-4-yl 4-[5-(2,2,3,3,4,4,4-heptafluorobutoxy)pentyl-1-oxy]benzoate (I.5.(HH) (S)) is described in [16, 17] and synthesis of (S)-4'-(1-ethylhexyloxycarbonyl)biphenyl-4-yl 4-[5-(2,2,3,3,4,4,4-heptafluorobutoxy)pentyl-1-oxy]benzoate (II.5.(HH) (S)) is presented in [18].

The X-ray diffraction experiment for the polycrystalline pristine samples (not melted after synthesis) was carried out with X'Pert PRO (PANalytical) diffractometer in the Bragg–Brentano geometry with the Cu K_α radiation. The diffraction patterns were collected in the 2θ = 2–30° range during heating from room temperature until the transition to isotropic liquid. The temperature was controlled using the TTK 450 (Anton Paar) stage. The XRD data analysis was performed in FullProf [19], PASCal [20, 21], and OriginPro.

The molecular modeling was performed in Gaussian 16 [22]. The conformational energy scans were carried out for isolated molecules and selected torsional angles with the semi-empirical PM7 method [23]. The lowest-energy conformations were further optimized by the DFT method (def2TZVPP basis set [24], B3LYP-D3(BJ) exchange-correlation functional [25–27]). The preparation and visualization of molecular models was done in Avogadro [28].

3. Results and discussion

3.1. Crystal unit cell

At room temperature, both compounds are in the crystal phases (Fig. 2), and the XRD patterns can be indexed in the orthorhombic and

TABLE I

Thermal expansion coefficients α_i and matrix of transition between the crystallographic directions and principal strain axes for the crystal phases of I.5.(HH) (S) and II.5.(HH) (S).

Compound	Axis	α_i ($\times 10^{-6}$) [K^{-1}]	a	b	c
I.5.(HH) (S)	x	$-231(4)$	1	0	0
	y	386(17)	0	1	0
	z	331(13)	0	0	1
	V	489(15)			
II.5.(HH) (S)	x	179(6)	0.7359	0	0.6771
	y	123(3)	0	1	0
	z	136(3)	-0.5485	0	0.8362
	V	442(4)			

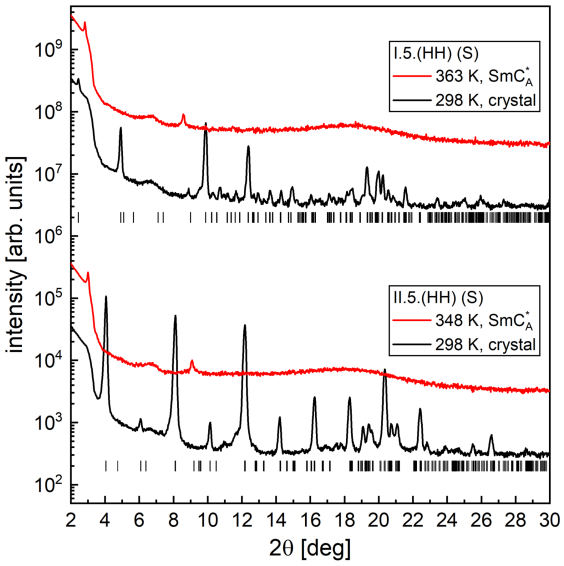

Fig. 2. X-ray diffraction patterns of I.5.(HH) (S) and II.5.(HH) (S) in their pristine crystal phases and after melting to the SmC^*_A phase. The vertical bars indicate the peak positions corresponding to the crystal unit cells mentioned in the main text. The wide maximum at $2\theta = 6$–7° is a background contribution.

monoclinic crystallographic system for I.5.(HH) (S) and II.5.(HH) (S), respectively. The unit cell sizes were determined by the Le Bail fitting method [29]. The lattice parameters in the room temperature for I.5.(HH) (S) are $a = 35.68(2)$ Å, $b = 17.23(2)$ Å, $c = 7.603(8)$ Å, $\alpha = \beta = \gamma = 90^\circ$ and for II.5.(HH) (S) are $a = 21.866(7)$ Å, $b = 4.834(6)$ Å, $c = 18.69(2)$ Å, $\beta = 92.73(9)^\circ$, $\alpha = \gamma = 90^\circ$. The parameter a for I.5.(HH) (S) is comparable with the molecule's length of 30–41 Å, based on the DFT results for various conformations. This indicates that the crystal phase of the pristine I.5.(HH) (S) sample very likely has a lamellar structure. The calculated length of the II.5.(HH) (S) molecule is 30–39 Å, which does not correspond to any lattice constant. Thus, the arrangement of molecules is likely not similar to that in the smectic phases. The differential scanning calorimetry results for pristine samples indicate that the enthalpy change at melting, which is equal to 18.0 kJ/mol for I.5.(HH) (S) [17], is much smaller than 27.8 kJ/mol for II.5.(HH) (S) [18]. This corresponds to the XRD results, which show that the lamellar crystal structure of I.5.(HH) (S) resembles more closely the smectic phase than the probably non-lamellar crystal structure of II.5.(HH) (S), therefore the enthalpy of melting is lower in the former compound.

The unit cell parameters, determined from the XRD patterns as a function of temperature (Fig. 3), were analyzed in the PASCal program, which enables the calculation of the coefficients of thermal expansion (CTEs) along the principal strain axes x, y, z [20, 21] (Table I). CTE in a given direction $i = x, y, z$ is defined as [20]

$$\alpha_i = \frac{1}{T}\left(\frac{l_i(T)}{l_i(0)} - 1\right), \tag{2}$$

where $l_i(T)$ is length (or volume, if the overall CTE is calculated) at temperature T. For I.5.(HH) (S), which crystallizes in the orthorhombic system, the principal axes overlap with the crystallographic directions a, b, c, and the transformation matrix between them is simply a unit matrix. As the b and c parameters deviate from the linear dependence above 318 K, only values from the 298–318 K range were used in calculations. The I.5.(HH) (S) compound in the crystal phase shows the positive expansion in the b and c directions, while along the a direction, CTE is negative. Another behavior is observed for the II.5.(HH) (S) crystal, which has positive CTEs along all directions. Despite significant differences in the anisotropy in thermal expansion, the volume CTE has similar values for both compounds.

3.2. Short-range order

The short-range order within the smectic layers appears in the diffraction patterns as a wide maximum with the middle at $2\theta \approx 18^\circ$. The same maximum is present after the transition to the isotropic liquid state. When plotted in the scattering vector space $q = 4\pi \sin(\theta)/\lambda$, the wide maximum has a Lorentzian shape [30, 31]

$$I(q) = \frac{I_0}{1 + \xi^2 (q - q_0)^2}, \tag{3}$$

where I_0 is the maximum height, q_0 is the maximum position, and ξ is the correlation length. The distance $w = q_0/\pi$, which corresponds approximately to the molecular width, is determined with an accuracy better than 0.01 Å (Fig. 4) and is within the

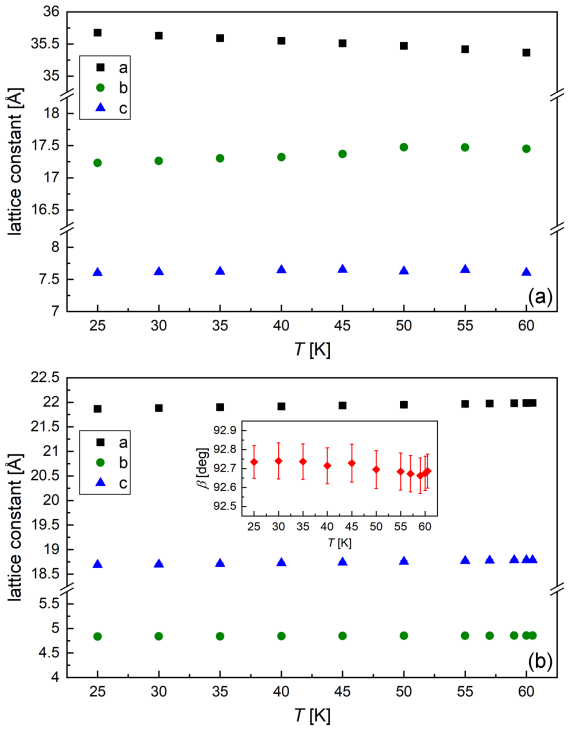

Fig. 3. Unit cell parameters for the crystal phases of I.5.(HH) (S) (a) and II.5.(HH) (S) (b).

4.76–4.99 Å range for I.5.(HH) (S) and 4.84–5.06 Å for II.5.(HH) (S). It is in agreement with slightly wider II.5.(HH) (S) molecules, due to the structure of their chiral center. Note that the presented w values are mean distances for each temperature, while the distribution of intramolecular distances is quite wide, and they may differ even by 0.5 Å between particular molecules. The mean w distance does not change significantly after the transition to isotropic liquid. The correlation length of the short-range order, determined with the accuracy of ca. 0.1–0.2 Å, decreases upon heating in the smectic phases and has an approximately constant value in isotropic liquid. It takes larger values for I.5.(HH) (S) than for II.5.(HH) (S), both in the smectic phases and isotropic liquid phase. Just above the Cr $\rightarrow$ SmC$^*_A$ transition temperature, at 341–348 K, the ξ value is equal to 6.7–7.1 Å for I.5.(HH) (S), while for II.5.(HH) (S) at lower temperatures 334.5–335.5 K, ξ equals 5.7–5.8 Å. A larger correlation length for I.5.(HH) (S) corresponds to the occurrence of the monotropic hexatic smectic phase formed by this compound upon overcooling [14], which was not observed for II.5.(HH) (S) [15]. The short-range correlations include only the nearest neighbors, as the ξ values are in the same order as the w distance. Correlation lengths obtained for other compounds in the smectic A or C phases are comparable with the results for I.5.(HH) (S) and II.5.(HH) (S) for some cases [31–33], but they can also be larger, above 10 Å [34, 35].

3.3. Smectic layer order

The lamellar order is present in the smectic phases, which corresponds to the low-angle sharp diffraction peaks. For the investigated compounds, the 1st and 3rd order peaks are visible, and the layer spacing (Fig. 5) was determined from the position of both of them using the Bragg equation

$$n\lambda = 2d\sin(\theta), \tag{4}$$

where n is the diffraction order, λ is the X-ray wavelength, d is the layer spacing, and θ is the peak position [36]. The layer spacing in the smectic phases of I.5.(HH) (S) is 1.8–2.1 Å larger than that of II.5.(HH) (S), which is caused by a longer chiral terminal chain of I.5.(HH) (S), as the tilt angle in both compounds deep in the SmC$^*_A$ phase is similar, i.e., 44.5° for I.5.(HH) (S) and 43° for II.5.(HH) (S) [13]. The SmC$^*_A$ $\rightarrow$ SmC* transition in I.5.HH (S) is only very weakly visible in the $d(T)$ plot as a discontinuous increase by 0.3 Å. For II.5.(HH) (S), no significant increase in d indicates the SmC$^*_A$ $\rightarrow$ SmA* transition. The previous results from other experimental methods [15] show that it is troublesome to detect the SmA* phase of this compound on heating.

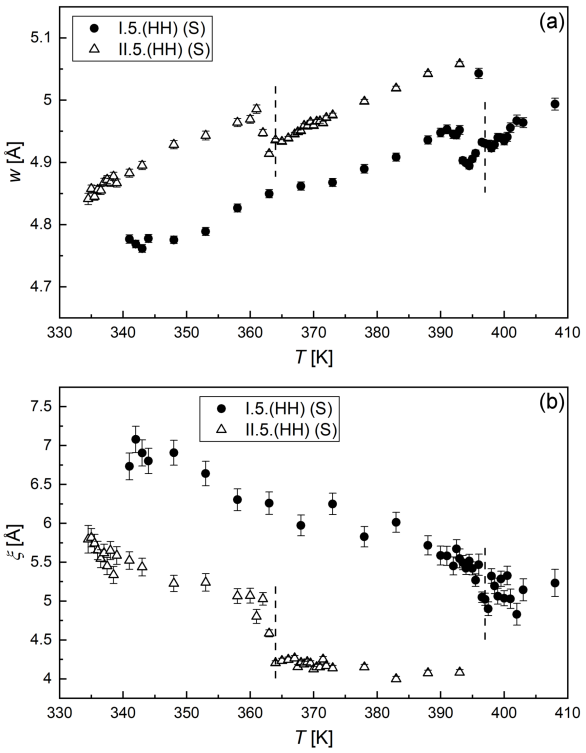

Fig. 4. Mean distance between molecules (a) and correlation length of the short-range order (b) determined from the XRD patterns. The vertical dashed lines indicate the smectic $\rightarrow$ isotropic liquid transition temperature for each compound.

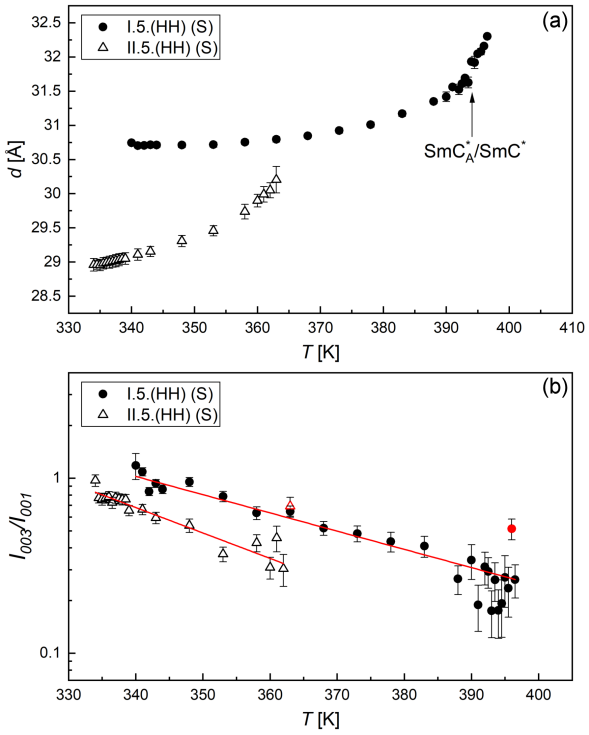

Fig. 5. Smectic layer spacing (a) and the ratio of the 1st and 3rd order peak from the lamellar order (b) determined from the XRD patterns. The Lorentz-polarization factor corrected the intensities in (b). Two outlier points in (b) close to the isotropization temperature were excluded from the linear fit.

The intensities of the 1st and 3rd order peaks are proportional to the τ_1 and τ_3 order parameters, respectively, describing the lamellar order. For the simplest, sinusoidal density wave, $1 > \tau_1 > 0$ and $\tau_m = 0$, where $m > 1$ [37]. The ratio of intensities of the 1st and 3rd order peak I_{003}/I_{001}, corrected by the Lorentz-polarization factor [38], is larger for I.5.(HH) (S) than for II.5.(HH) (S), which means that in the former compounds, there is a larger deviation from the sinusoidal density wave. The I_{003}/I_{001} ratio for both compounds increases with decreasing temperature in an exponential manner, which is visible as a linear dependence when I_{003}/I_{001} is plotted in the logarithmic scale (Fig. 5b); only the points close to the transition to the isotropic liquid show some deviations from this dependence.

3.4. Tilt angle

The conformational energy scans for a few torsional angles in the I.5.(HH) (S) and II.5.(HH) (S) molecules were previously presented in [14, 15] and were used for the interpretation of the dielectric relaxation processes. New conformations

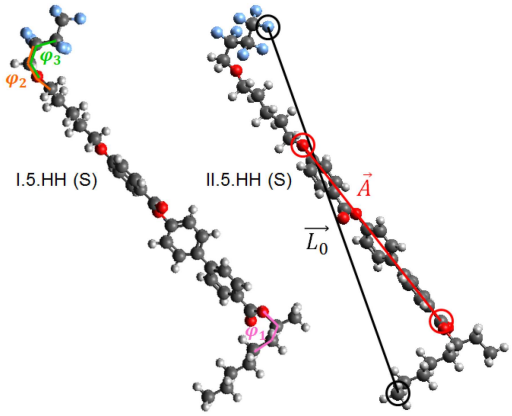

Fig. 6. Molecular model optimized with the DFT method ($\varphi_1 \approx 62$–$63.5°$, $\varphi_2 \approx 110°$, $\varphi_3 \approx 295°$). For I.5.(HH) (S), the φ_1, φ_2 and φ_3 angles are indicated. For II.5.(HH) (S), the $\boldsymbol{L_0}$ and $\boldsymbol{A}$ vectors are defined. The molecular length is obtained as $L = L_0 + 3.22$ Å, and the shape parameter $\delta\Theta$ is equal to an angle between $\boldsymbol{L_0}$ and $\boldsymbol{A}$.

were included to determine the tilt angle from the XRD results in this study. The molecular models from [14, 15] were used as the starting point for new calculations. The semi-empirical PM7 method is useful for performing quick scans of the conformational energy as a function of a given torsional angle, because the calculation for an isolated molecule consisting of 91 atoms, as it is for both considered compounds, lasts less than one minute. The amount of possible molecular conformations is large. Therefore, only selected torsional angles can be investigated in a reasonable time. These torsional angles, indicated in Fig. 6, are the C–C–C*–O angle φ_1 in the chiral center, as well as the C–O–C–C angle φ_2 and O–C–C–C angle φ_3 in the fluorinated part of the achiral chain. They were chosen because each of them significantly influences the length and shape of molecules. The PM7 scans for φ_1 and φ_3 show three local minima in energy, while for φ_2 there are two local minima (Fig. 7). Only the φ_1 scans differ slightly between I.5.(HH) (S) and II.5.(HH) (S), while the φ_2 and φ_3 scans for both compounds overlap, as these angles are far from the chiral center. In the next step, the DFT calculations, each lasting up to 12 h, were performed for conformations corresponding to the local minima in energy, without any constraints in the torsional angles. The DFT method reveals a third local minimum in energy for φ_2, and in some cases, the φ values in the optimized models differ slightly from the results of the simpler PM7 method. For each considered torsional angle, there are local minima in energy corresponding to an antiperiplanar conformation ($\varphi \approx 180°$) and two *gauche* conformations. Eventually, 27 molecular models with various values of φ_1, φ_2, and φ_3 were optimized for each compound (Table II).

TABLE II

Tilt angle Θ in the SmC^*_A phase of I.5.(HH) (S) and II.5.(HH) (S) obtained from the experimental smectic layer spacing at 340 K and 334 K, respectively, and molecular models optimized by the DFT method. For each conformation, the relative energy ΔE is given together with the values of torsional angles ϕ_1, ϕ_2, ϕ_3. The **bold** font indicates results that are in agreement with the 2° error with the experimental tilt angle [13] at corresponding temperatures, namely 44.5° for I.5.(HH) (S) and 42° for II.5.(HH) (S).

I.5.(HH) (S)					II.5.(HH) (S)				
ΔE [kJ/mol]	φ_1 [deg]	φ_2 [deg]	φ_3 [deg]	Θ [deg]	ΔE [kJ/mol]	φ_1 [deg]	φ_2 [deg]	φ_3 [deg]	Θ [deg]
0.02	62.3	78.7	50.3	**46.2(1)**	0	63.5	78.6	50.2	45.9(4)
2.81	62.4	88.6	175.6	**44.5(1)**	2.82	63.3	88.4	175.2	**41.7(3)**
4.23	62.3	109.7	294.7	**42.8(2)**	4.27	63.5	109.6	294.6	**41.2(5)**
1.70	62.4	181.3	58.5	34.4(1)	1.68	63.4	181.2	58.4	45.8(3)
3.95	62.4	180.0	180.1	**42.9(1)**	3.95	63.5	180.1	179.9	44.6(3)
1.67	62.4	178.8	301.4	**46.2(1)**	1.68	63.4	179.0	301.5	50.3(3)
4.24	62.2	250.5	65.6	–	4.26	63.4	250.6	65.4	24.9(7)
2.83	62.4	271.5	184.7	35.9(1)	2.84	63.4	269.8	183.4	35.4(3)
0	62.2	281.3	309.9	15.9(3)	0.04	63.5	281.5	309.8	33.9(5)
1.45	174.4	78.8	50.5	51.2(1)	9.99	178.6	78.7	50.4	53.1(3)
4.23	174.25	90.1	176.8	50.3(1)	12.79	178.5	89.7	176.2	51.7(3)
5.69	174.4	109.9	294.6	49.8(1)	14.24	178.7	109.9	294.5	51.7(3)
3.12	174.3	181.0	58.5	**43.7(1)**	11.66	178.7	181.3	58.5	45.4(3)
5.38	174.3	180.2	180.0	47.8(1)	13.93	178.6	180.3	180.1	49.2(2)
3.11	174.2	178.5	301.6	50.8(1)	11.68	178.7	180.5	301.5	52.5(3)
5.67	174.3	250.4	65.5	32.2(1)	14.24	178.8	250.3	65.6	33.0(3)
4.24	174.4	271.0	184.4	**44.6(1)**	12.80	178.7	271.6	184.8	45.7(3)
1.43	174.3	281.2	309.8	34.8(1)	10.00	178.8	281.2	309.8	36.3(3)
1.90	300.8	78.7	50.0	**43.0(2)**	1.86	297.5	78.7	50.0	49.0(4)
4.72	300.9	89.0	175.8	40.0(1)	4.67	297.5	87.9	174.9	44.9(3)
6.15	300.6	109.4	294.5	35.8(2)	6.14	297.5	109.6	294.6	45.0(4)
3.58	300.9	181.1	58.5	38.4(1)	3.55	297.5	181.3	58.4	**42.9(3)**
5.85	300.8	180.3	180.1	41.1(1)	5.85	297.5	179.8	179.9	45.4(3)
3.58	300.8	178.9	301.5	46.6(1)	3.55	297.6	178.8	301.5	50.6(3)
6.16	300.8	250.7	65.4	–	6.13	297.5	250.7	65.4	20.0(7)
4.74	301.0	271.5	184.7	31.3(1)	4.71	297.5	270.4	183.7	37.2(3)
1.92	300.8	281.4	309.7	18.3(3)	1.89	297.6	281.3	309.7	30.0(5)

The tilt angle Θ was calculated using formula (1). The smectic layer spacing determined just above the melting of the crystal phase, $d = 30.75(3)$ Å for I.5.(HH) (S) and 29.0(1) Å for II.5.(HH) (S), was inserted in this formula. The molecular length L was defined as the distance between the terminal C atom from the chiral chain and the terminal F atom from the achiral chain, plus the non-bonded C–F distance 3.22 Å [39]. For the sake of unambiguity of L, the same F atom, which follows the positions of the C atoms in the achiral chain, was selected for all conformations. There are various approaches to calculate the shape parameter $\delta\Theta$ [8]. In this work, $\delta\Theta$ was defined simply as an angle between the C–F vector related to the molecular length and the C–O vector, where C is located in the COO group between the biphenyl ring and the chiral center, and O is adjacent to the benzene ring (see Fig. 6). The final values of Θ obtained from the XRD and DFT results are presented in Table II. The uncertainties in Θ given in parentheses are related to uncertainties in d, which do not exceed 1°. However, for practical purposes, an agreement within the ±2 error with experimental Θ from [13] is satisfactory, and the bold font in Table II denotes such values. One can see that for both compounds, a good agreement is obtained for conformations where $\varphi_1 \approx 62$–$63.5°$ and $\varphi_2 \approx 89°$, $\varphi_3 \approx 175$–$176°$ or $\varphi_2 \approx 110°$, $\varphi_3 \approx 295°$. Thus, these conformations, among the considered ones, are most likely exhibited by the real molecules in the SmC^*_A phase.

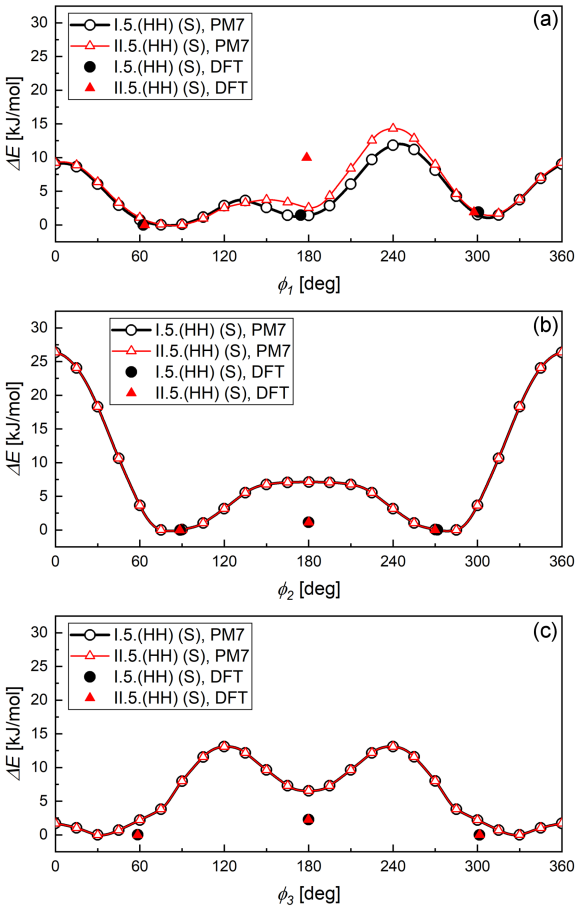

Fig. 7. Conformational energy of I.5.(HH) (S) and II.5.(HH) (S) molecules as a function of torsional angles, defined in the main text, calculated with the PM7 and DFT methods.

4. Conclusions

The structural parameters of I.5.(HH) (S) and II.5.(HH) (S), with chiral centers based on (S)-(+)-2-octanol and (S)-(+)-3-octanol, in the crystal and smectic phases were compared using the X-ray diffraction patterns registered as a function of temperature. The main conclusions are as follows:

- In the pristine samples, I.5.(HH) (S) crystallizes in the orthorhombic system, while II.5.(HH) (S) crystallizes in the monoclinic system. I.5.(HH) (S) exhibits the strong anisotropy of CET, which is negative along the *a*-axis and positive along the *b*- and *c*-axes. For II.5.(HH), CETs are positive in all directions.
- The average distance between molecules is smaller and the correlation length describing the short-range order within the smectic layers is larger for I.5.(HH) (S) than for II.5.(HH) (S).
- The smectic layer spacing and deviation from the sinusoidal density wave is larger for I.5.(HH) (S) than for II.5.(HH) (S). In both compounds, the ratio of the 3rd and 1st diffraction peaks decreases exponentially with increasing temperature.
- Among the set of 27 conformations obtained by DFT calculations, the most probable are these with $\varphi_1 \approx 62$–$63°$ and $\varphi_2 \approx 89°$, $\varphi_3 \approx 175$–$176°$ or $\varphi_2 \approx 110°$, $\varphi_3 \approx 295°$, as they lead to good agreement with the experimental tilt angle (measured by the electro-optic method in [13]) for both compounds. Further XRD experiments will show if the conformations that are considered most probable for I.5.(HH) (S) and II.5.(HH) (S) agree with the optical tilt angle for similar compounds.

Acknowledgments

We gratefully acknowledge Poland's high-performance infrastructure PLGrid Academic Computer Centre Cyfronet AGH for providing computer facilities and support within computational grant no. plgmolkryst-8.

References

[1] G. Vertogen, W.H. de Jeu, *Thermotropic Liquid Crystals, Fundamentals*, Springer-Verlag, Berlin 1988.

[2] J. Als-Nielsen, J.D. Litster, R.J. Birgeneau, M. Kaplan, C.R. Safinya, A. Lindegaard-Andersen, S. Mathiesen, *Phys. Rev. B* **22**, 312 (1980).

[3] J.P.F. Lagerwall, F. Giesselmann, *ChemPhysChem* **7**, 20 (2006).

[4] K. D'havé, P. Rudquist, S.T. Lagerwall, H. Pauwels, W. Drzewiński, R. Dąbrowski, *Appl. Phys. Lett.* **76**, 3528 (2000).

[5] R. Dąbrowski, J. Gąsowska, J. Otón, W. Piecek, J. Przedmojski, M. Tykarska, *Displays* **25**, 9 (2004).

[6] J.T. Mills, H.F. Gleeson, J.W. Goodby, M. Hird, A. Seed, P. Styring, *J. Mater. Chem.* **8**, 2385 (1998).

[7] W. Piecek, Z. Raszewski, P. Perkowski, J. Przedmojski, J. Kędzierski, W. Drzewiński, R. Dąbrowski, J. Zieliński, *Ferroelectrics* **310**, 125 (2004).

[8] A. Deptuch, T. Jaworska-Gołąb, M. Dziurka, J. Hooper, M. Srebro-Hooper, M. Urbańska, M. Tykarska, M. Marzec, *Phys. Rev. E* **107**, 034703 (2023).

[9] W. Tomczyk, M. Marzec, E. Juszyńska, R. Dąbrowski, D. Ziobro, S. Wróbel, M. Massalska-Arodź, *Acta Phys. Pol. A* **124**, 949 (2013).

[10] A. Drzewicz, E. Juszyńska-Gałązka, W. Zając, M. Piwowarczyk, W. Drzewiński, *J. Mol. Liq.* **319**, 114153 (2020).

[11] K. Drużbicki, E. Mikuli, A. Kocot, M.D. Ossowska-Chruściel, J. Chruściel, S. Zalewski, *J. Phys. Chem. A* **116**, 7809 (2012).

[12] P. Perkowski, Z. Raszewski, J. Kędzierski, J. Rutkowska, W. Piecek, J. Zieliński, S. Kłosowicz, *Ferroelectrics* **276**, 279 (2002).

[13] M. Urbańska, P. Morawiak, M. Senderek, *J. Mol. Liq.* **328**, 115378 (2021).

[14] A. Deptuch, M. Jasiurkowska-Delaporte, W. Zając, E. Juszyńska-Gałązka, A. Drzewicz, M. Urbańska, *Phys. Chem. Chem. Phys.* **23**, 19795 (2021).

[15] A. Deptuch, A. Lelito, E. Juszyńska-Gałązka, M. Jasiurkowska-Delaporte, M. Urbańska, *Phys. Chem. Chem. Phys.* **25**, 12379 (2023).

[16] M. Żurowska, R. Dąbrowski, J. Dziaduszek, K. Czupryński, K. Skrzypek, M. Filipowicz, *Mol. Cryst. Liq. Cryst.* **495**, 145/[497] (2008).

[17] M. Żurowska, R. Dąbrowski, J. Dziaduszek et al., *J. Mater. Chem.* **21**, 2144 (2011).

[18] M. Żurowska, M. Filipowicz, M. Czerwiński, M. Szala, *Liq. Cryst.* **46**, 299 (2019).

[19] J. Rodríguez-Carvajal, *Phys. B Condens. Matter* **192**, 55 (1993).

[20] M.J. Cliffe, A.L. Goodwin, *J. Appl. Cryst.* **45**, 1321 (2012).

[21] M. Lertkiattrakul, M.L. Ewans, M.J. Cliffe, *J. Open Source Softw.* **8**, 5556 (2023).

[22] M.J. Frisch, G.W. Trucks, H.B. Schlegel et al., Gaussian 16, Revision C.01, Gaussian Inc., Wallingford (CT) 2019.

[23] J.J.P. Stewart, *J. Mol. Model.* **19**, 1 (2013).

[24] F. Weigend, R. Ahlrichs, *Phys. Chem. Chem. Phys.* **7**, 3297 (2005).

[25] C. Lee, W. Yang, R.G. Parr, *Phys. Rev. B* **37**, 785 (1988).

[26] A.D. Becke, *J. Chem. Phys.* **98**, 5648 (1993).

[27] S. Grimme, S. Ehrlich, L. Goerigk, *J. Comput. Chem.* **32**, 1456 (2011).

[28] M.D. Hanwell, D.E. Curtis, D.C. Lonie, T. Vandermeersch, E. Zurek, G.R. Hutchison, *J. Cheminform.* **4**, 17 (2012).

[29] A. Le Bail, H. Duroy, J.L. Fourquet, *Mater. Res. Bull.* **23**, 447 (1988).

[30] J. Budai, R. Pindak, S.C. Davey, J.W. Goodby, *J. Phys. Lett.* **45**, 1053 (1984).

[31] J. Yu, Z. Chen, R. Teerakapibal, C. Benmore, R. Richert, L. Yu, *J. Chem. Phys.* **156**, 084504 (2022).

[32] W. Tomczyk, M. Marzec, E. Juszyńska-Gałązka, D. Węgłowska, *J. Mol. Struct.* **1130**, 503 (2017).

[33] A. Różycka, A. Deptuch, T. Jaworska-Gołąb, D. Węgłowska, M. Marzec, *Phase Trans.* **91**, 159 (2018).

[34] K. El Guermai, M. Ayadi, K. El Boussiri, *Acta Phys. Pol. A* **94**, 779 (1998).

[35] B.M. Ocko, A.R. Kortan, R.J. Birgeneau, J.W. Goodby, *J. Phys.* **45**, 113 (1984).

[36] W. Massa, *Crystal Structure Determination*, Springer-Verlag, Berlin 2000.

[37] Y. Takanishi, A. Ikeda, H. Takezoe, A. Fukuda, *Phys. Rev. E* **51**, 400 (1995).

[38] B.B. He, in: C.J. Gilmore, J.A. Kaduk, H. Schenk, *International Tables for Crystallography*, Vol. B, 2019, p. 130.

[39] R.S. Rowland, R. Taylor, *J. Phys. Chem.* **100**, 7384 (1996).